

Journal of Materials Chemistry C

Accepted Manuscript



This is an *Accepted Manuscript*, which has been through the Royal Society of Chemistry peer review process and has been accepted for publication.

Accepted Manuscripts are published online shortly after acceptance, before technical editing, formatting and proof reading. Using this free service, authors can make their results available to the community, in citable form, before we publish the edited article. We will replace this *Accepted Manuscript* with the edited and formatted *Advance Article* as soon as it is available.

You can find more information about *Accepted Manuscripts* in the [Information for Authors](#).

Please note that technical editing may introduce minor changes to the text and/or graphics, which may alter content. The journal's standard [Terms & Conditions](#) and the [Ethical guidelines](#) still apply. In no event shall the Royal Society of Chemistry be held responsible for any errors or omissions in this *Accepted Manuscript* or any consequences arising from the use of any information it contains.

Poly(3-butylthiophene) Nanowires Inducing Crystallization of Poly(3-hexylthiophene) for Enhanced Photovoltaic Performance

Lin Zhang¹, Weihua Zhou^{*1,2}, Jiangman Shi¹, Ting Hu¹, Xiaotian Hu¹, Yong Zhang¹,
Yiwang Chen^{1,2}

¹School of Materials Science and Engineering/Institute of Polymers, Nanchang University, 999 Xuefu Avenue, Nanchang 330031, China; ²Jiangxi Provincial Key Laboratory of New Energy Chemistry, College of Chemistry, Nanchang University, 999 Xuefu Avenue, Nanchang 330031, China

Abstract: The poly(3-butylthiophene) nanowires (P3BT-nw) were incorporated into poly(3-hexylthiophene) (P3HT) and [6,6]-phenyl-C61-butyric acid methyl ester (PCBM) to modulate the morphology of the active layer for enhanced photovoltaic performance. The P3BT-nw were found to induce the crystallization of P3HT as revealed by X-ray diffraction (XRD) and differential scanning calorimetry (DSC). Furthermore, the existence of P3BT-nw facilitated the aggregation of PCBM molecules into larger clusters as revealed by the grazing-incidence small angle X-ray scattering (GISAXS). The power conversion efficiency of the ternary blend device could reach to the highest value of 4.2% at P3BT-nw weight percentage of 7 wt%, in comparison with the pristine P3HT:PCBM system of 3.0%. The improved performance should be associated with the enhanced hole and electron mobilities, due to the formation of interconnected pathways along the crystallites of P3HT and P3BT-nw for efficient long-range charge transport.

Keywords: nanowire; crystallization; aggregation; grazing-incidence small angle X-ray scattering

* Corresponding author. Tel.: +86 791 83969562; fax: +86 791 83969561. *E-mail address:* zhouweihua@ncu.edu.cn (W. Zhou).

Introduction

Polymer solar cells (PSCs) have drawn significant attention in the past decades due to their light weight, low-temperature solution processing, good mechanical flexibility, and large area manufacturing.¹⁻³ The power conversion efficiency (PCE) of PSCs with a bulk heterojunction (BHJ) has reached to 10%, by designing the novel donor and acceptor materials, using efficient device structure, tuning interfacial materials, and applying new preparation technology.⁴⁻¹⁴ One of the most widely studied systems in PSCs is a blend of regioregular poly(3-hexylthiophene) (P3HT) and [6,6]-phenyl-C61-butyric acid methyl ester (PCBM) with the efficiency of 3-5%,¹⁵⁻¹⁶ and the primary method of improving efficiency has been the optimization of the two-phase nanostructure of the donor and acceptor materials.¹⁷⁻¹⁸ Various approaches have been used to control the nanoscale film morphology, including thermal and solvent annealing,¹⁹⁻²⁰ use of mixed solvents as a mean to control aggregation of the polymer,²¹ incorporation of a third additive such as high-boiling-point 1,8-diiodooctane (DIO),²² amphiphilic molecules of thiophene-C60 derivatives,²³ rod-coil copolymers as interfacial compatibilizers,²⁴ liquid crystalline molecules,²⁵ narrow band gap polymer²⁶, dyes,²⁷⁻²⁸ semiconductor nanocrystals,²⁹ and so on. Unlike typical inorganic semiconductors with a crystalline structure, the charge dynamics of P3HT are severely limited by the presence of amorphous portions between the ordered crystalline regions. The formation of interconnected pathways along the crystallites of P3HT is desired to ensure highly efficient long-range charge transport in P3HT:PCBM system.³⁰

Recently, the self-assembled 1D nanostructures of P3HT have been shown to largely enhance the crystallinity, mechanical flexibility, and the speed of charge transport, as compared with the 2D thin film counterparts.³¹⁻³³ The directional transport of the holes along P3HT nanowires may lead to increased carrier mobility and remarkable improvement in PCE value even without any annealing process.³⁴ There are numerous methods to prepare the P3HT nanowires, including the ultrasonic-assisted nanowires formation in co-solvent systems,³⁵⁻³⁶ UV irradiation in chloroform and toluene,³⁷

self-seeded growth of nanowires by a cycle of cooling and heating in solutions³³ and so on. It should be noted that the growth of P3HT nanowires is difficult in 1,2-dichlorobenzene (ODCB) which is demonstrated to be the optimized solvent for P3HT and PCBM system, due to the similar solubility parameter for P3HT and ODCB. In contrast, the poly(3-butylthiophene) nanowires (P3BT-nw) were easy to obtain in the ODCB solution, simply via cooling from 90-100 °C to room temperature in dark environment as reported by Jenekhe.³⁸ They have performed a systematic study of the P3BT-nw using as the donor and PCBM as the acceptor in the photovoltaic applications. Although the hole mobility of P3BT is 9 times lower than that of P3HT, the solar cell device based on P3BT-nw and PC₇₁BM could reach to an efficiency of 3.0%, which is comparable to the P3HT:PC₇₁BM system of 3.0%. By optimizing the donor and acceptor ratio and combining of thermal annealing, the PCE reached to the highest value of 3.35%.³⁹

In conclusion, incorporation of polymer semiconductor nanowires into the BHJ solar cell exhibits many advantages: (a) the polymer nanowires with widths of 10-20 nm and lengths of microns have sizes that are perfectly matched to the exciton diffusion lengths; (b) high carrier mobilities and high absorption coefficient are achieved because of the high crystallinity of the self-assembled nanowires; (c) it avoids the difficulties of blend phase-separation phenomena, including domain coarsening and time-dependent instability.⁴⁰ As far as we are concerned, the incorporation of P3BT-nw as a third additive into the conventional P3HT:PCBM system has not been reported. Additionally, the influence of P3BT-nw on the crystallization of P3HT and the aggregation of PCBM is not known.

In this work, P3BT-nw were incorporated into P3HT:PCBM system via solution blending in ODCB. The P3BT-nw are supposed to serve as the template to induce the crystallization of P3HT and play the role of bridge between different P3HT crystalline domains to offer multi-charge-transfer channels for more efficient charge separation and transfer, which eventually leads to the increase of photovoltaic performance. The

crystallization of P3HT in the presence of P3BT-nw, as well as the relationship between morphology of the P3HT:P3BT-nw:PCBM ternary system and performance of the solar cells has been extensively studied. The approach was demonstrated to largely increase the short-circuit current (J_{sc}) from 7.79 mA/cm² to 9.84 mA/cm² and fill factor (FF) from 65.1% to 70.1%, thereby enhance the power conversion efficiency from 3.0% to 4.2% in polymer and fullerene bulk heterojunction solar cells. This article presented a novel method to build an interconnected pathway of conjugated polymers with 3D network formation from solution by the nanowire induced crystallization.

Experimental section

Materials

Regioregular P3HT ($M_w = 48300 \text{ g}\cdot\text{mol}^{-1}$, head-to-tail regioregularity > 90%) and PC₆₁BM (99.5% purity) used in this study were purchased from Rieke Metals, Inc. and Nano-C, respectively. P3BT ($M_w = 15000 \text{ g}\cdot\text{mol}^{-1}$, head-to-tail regioregularity of 97%) was purchased from Aldrich. Poly(3,4-ethylenedioxythiophene):poly(styrenesulfonate) (PEDOT:PSS) (Clevios, Heraeus PVP Al 4083) was obtained from Bayer Inc, whereas indium tin oxide (ITO) glass was purchased from Delta Technologies Limited. 1,2-Dichlorobenzene (ODCB) was purchased from Aldrich. All the reagents were used directly as received without further purification.

Preparation of P3BT-nw

3 mL and 1 mL 1,2-dichlorobenzene (ODCB) solvent were added into two 5 mL bottles containing 6 mg and 10 mg P3BT, respectively. The P3BT suspensions (2 mg/mL and 10 mg/mL) were stirred at 90 °C for 10 h until P3BT was completely dissolved. Then, the hot solution was put in a dark environment for more than 24 hours at room temperature to allow P3BT chains to self-assemble. The original orange brown color of the solution changed to dark violet after the formation of P3BT-nw as a dispersion. The nanowires did not dissolve in ODCB by dilution, but it can be re-dissolved by heating treatment upon 90 °C. The P3BT solution (2 mg/mL and 10 mg/mL) was prepared by stirring at 90 °C for 10 h until P3BT was completely dissolved. The solution was used immediately in order to avoid the formation of nanowires.

Preparation of P3HT:P3BT-nw:PCBM ternary blends

The P3HT (60 mg) and PCBM (60 mg) were charged into two bottles, followed by the addition of 1.5 mL ODCB to obtain the 40 mg/mL P3HT and 40 mg/mL PCBM solution, respectively. Then, the suspensions were stirred in glovebox at 60 °C overnight. The P3BT-nw suspension, P3HT solution and PCBM solution were mixed

together (1:0:1, 0.97:0.03:1, 0.93:0.07:1, 0.9:0.1:1, 0.75:0.25:1, 0.5:0.5:1 of P3HT:P3BT-nw:PCBM in weight ratio) to obtain the ternary blend solution. The detailed weight or volume fraction of the ternary blend solution composing of P3BT-nw suspension, P3HT solution, PCBM solution and ODCB were shown in the supporting information (**Table S1**). Furthermore, the P3HT:P3BT:PCBM blends were prepared simply by mixing the solution together in the same weight ratio of P3HT:P3BT-nw:PCBM blends.

Device fabrication

The desired geometric configuration of indium tin oxide (ITO)-coated glass substrates were patterned by etching. The ITO glass substrates were cleaned by detergent, deionized water and isopropyl alcohol sequentially with ultrasound treating and dried by nitrogen flow, followed by UV treatment for 20 min. The cleaned ITO glass substrates were covered by spin coating with a layer of PEDOT:PSS (40 nm), drying at 140 °C for 20 min in air, and transferring into a nitrogen-filled glovebox. The P3HT:PCBM blends with different weight percentage of P3BT-nw or P3BT were spin-coated onto the top of PEDOT:PSS layer producing a 120 nm thick active layer and annealed at 150 °C for 10 min on hotplate in nitrogen-filled glovebox. Finally, 0.7 nm LiF and 100 nm Al were deposited on top of active layer by thermal evaporation through a shadow mask at a pressure of approximately 10^{-6} Torr as an electrode.

Characterization

Differential scanning calorimetry (DSC) was used to determine phase-transition temperatures on a TA DSC Q2000 differential scanning calorimeter with a constant heating/cooling rate of 10 °C/min. The corresponding melting temperature (T_m), melting enthalpy (ΔH_m), crystallization temperature (T_c) and crystallization enthalpy (ΔH_c) were measured. The preparation of the blends using for DSC analysis was described in the supporting information (**Table S2**). X-ray diffraction (XRD) study were recorded on a Bruker D8 Focus X-ray diffractometer with a copper target ($\lambda=1.54$ Å). The ultraviolet-visible (UV) spectra of the samples were recorded on a

PerkinElmer Lambda 750 spectrophotometer. Fluorescence measurement for photoluminescence (PL) of the polymers was carried out on a Hitachi F-7000 PC spectrofluorophotometer with a xenon lamp as the light source. The atomic force microscopy (AFM) images were measured on a nanoscope III A (Digital Instruments) scanning probe microscope using the tapping mode. The morphology of the films was conducted by employing transmission electron microscopy (TEM) (JEM-2010 HR) with an accelerating voltage of 200 kV. Photocurrent/voltage (J/V) curves were recorded using a Keithley 2400 Source Meter under 100 mW/cm^2 simulated AM 1.5 G irradiation (Abet Solar Simulator Sun2000) and in the dark. The current-voltage characterization was recorded by using a Keithley 2400 Source Meter. Grazing-incidence small-angle X-ray scattering (GISAXS) measurements were performed at the Shanghai Synchrotron Radiation Facility (SSRF) on the BL16B1 beamline using a photon energy of 10 keV with a sample to detector distance of approximately 2025 mm. The incident angle was set to 0.4° , which was above the critical angles of P3HT and PCBM and therefore the structure of the full film thickness was detected. The GISAXS signal was shielded with a rod-like beam stop.

Results and discussion

The P3BT-nw were prepared as dispersions by solution-phase self-assembly similar to the previously reported method.³⁸ As shown in **Figure 1a**, the pristine P3BT solution is orange brown, in contrast to the dark violet P3BT-nw suspension in ODCB. The UV-vis absorption profile of the original P3BT solution is different from that of P3BT-nw suspension. In addition to the absorption maximum (λ_{\max}) of the P3BT-nw suspension ($\lambda_{\max} = 494$ nm) which is red-shifted from the P3BT solution ($\lambda_{\max} = 457$ nm), two additional lower-energy shoulder peaks at 564 nm and 615 nm are characteristic of the crystalline P3BT.³⁸ The absorption spectra of the spin-coated films of pristine P3BT and P3BT-nw are also presented in **Figure 1a**. In contrast to the solution state, the maximum absorption peaks in the solid-state films for both P3BT and P3BT-nw exhibit obvious red-shift. The shoulder peak at about 615 nm in P3BT-nw film is stronger than that in P3BT film and solution, showing that the crystallinity of P3BT-nw is higher than P3BT. Furthermore, the AFM images of the spin-coated films from original P3BT solution and P3BT-nw suspension are illustrated in **Figure 1b** and **Figure 1c**, respectively. It is noted that the specimen from the P3BT-nw suspension exhibits interconnected structures, attributing to the formation of nanowires. However, unobvious nanowires could be noticed in the sample from original P3BT solution. The topography images of P3BT and P3BT-nw films are shown in **Figure S1**. It is revealed that the P3BT-nw have been successfully obtained based on the color and absorption change in solution as well as the morphology variation in films.

In order to explore the effect of P3BT-nw on the crystallization behavior of P3HT, the binary blends at different P3BT-nw weight ratios were prepared via the solution blending method. **Figure 2a** shows the X-ray spectra of the P3HT:P3BT-nw blends, and one or two intense and sharp diffraction peaks contributing to P3HT or P3BT could be noticed. For the pristine P3HT and P3HT:P3BT-nw blends, the diffraction peak at 5.48° assigned to the (100) diffraction of P3HT remains almost the same, and the lamellar spacing of P3HT crystallites is calculated to be about 1.61 nm according

to the Bragg equation. The shape of the reflection peaks is found to be dependent on the P3BT-nw weight percentage. By increasing of P3BT-nw content from 3 wt% to 10 wt%, the reflection peak of P3HT becomes stronger, illustrating of higher crystallinity. Moreover, the Grazing incident X ray diffraction (GIXRD) spectra of the films are shown in **Figure S2**. The relative intensity of (100) and (200) diffraction peaks attributing to P3HT become stronger upon incorporation of P3BT-nw, demonstrating that P3BT-nw could induce the crystallization of P3HT.

To further investigate the effect of P3BT-nw on the crystal size of P3HT, the crystalline correlation length (CCL) of P3HT and P3BT was calculated from Scherrer's equation by fitting the diffraction peaks:

$$CCL = \frac{2\pi}{FWHM} \quad (1)$$

where FWHM is the full-width-at-half-maximum of the fitted Pseudo-Voigt function. The CCL is a measure of crystallite size and/or perfection.⁴¹ The calculated parameters from XRD are shown in **Figure S3** and **Table S3**. The CCL value for P3HT decreases from 9.10 nm to 7.57 nm as P3BT-nw weight percentage reaches to 50 wt%. It is concluded that the P3BT-nw could induce the P3HT to form crystals in smaller size.

The interactions between P3BT-nw and P3HT were further investigated by DSC analysis. On the DSC heating curves, the melting peaks contributing to P3HT and P3BT could be noticed for the binary blends (**Figure 2b**). The T_m of P3HT decreases gradually from 228.4 °C to 218.1 °C as the P3BT-nw content increasing to 50 wt% (**Table 1**). The melting enthalpy of P3HT almost increases upon adding more P3BT-nw. In addition, the T_m of P3BT increases from 272.6 °C to 285.8 °C, accompanied by the increase of melting enthalpy from 5.0 J/g to 10.4 J/g for the blend containing 10 wt% P3BT-nw and pristine P3BT-nw, respectively. As cooling from the melting state, the crystallization temperature and enthalpy of P3HT reaches to the highest value of 182.8 °C and 11.3 J/g at P3BT content of 10 wt% (**Figure 2c**). The

P3BT-nw at low weight percentage facilitates the crystallization of P3HT as cooling from melting state. Moreover, the crystallization peak of P3HT becomes less obvious with T_c value showing of no significant change at P3BT-nw content above 25 wt%. In contrast, both of the crystallization temperature and enthalpy values for P3BT depresses at the existence of P3HT, due to the dilution effect of P3HT.

It is generally accepted that the melting temperature of a crystalline polymer is mainly related with the lamellar thickness of the crystals.⁴² As revealed by the XRD result, the P3BT-nw is believed to induce crystallization of P3HT during the solvent evaporation process, leading to the formation of thinner and smaller P3HT crystallites due to the existence of large amount of P3BT-nw nucleating point. Therefore, the T_m of P3HT depresses in the blends as P3BT-nw content increasing, attributing to the formation of thinner lamellae. Additionally, the melting enthalpy value could indirectly represent the crystallinity of the polymers, and the enhanced ΔH_m value for the P3HT component reveals that the P3BT-nw (below 10 wt%) does induce the crystallization of more P3HT chains. The simulative model that P3BT-nw induce the crystallization of amorphous P3HT chains serving as the nucleating agent was shown in **Figure S4**.

The X-ray spectra of the P3HT:P3BT-nw:PCBM ternary blend is shown in **Figure 3a**, and the corresponding parameters of lamellar spacing and CCL value are illustrated in **Figure S5** and **Table S4**. The position of P3HT (100) peak remains unchanged as the P3BT-nw content reaches to 10 wt%, and the peak slightly shifts to higher 2θ value at P3BT-nw content of 25 wt% and 50 wt%. Moreover, the intensity of the diffraction peak for P3HT gradually increases upon the incorporation of P3BT-nw, and the position of P3BT diffraction peaks remains constant. In the ternary blends, the P3BT-nw is supposed to play the role of nucleating agent to induce P3HT crystallization.

Figure 3b displays the UV-vis absorption spectrum of P3HT:P3BT-nw:PCBM ternary

blend films at different content of P3BT-nw. The spectrum of the pristine P3HT film shows a peak at 510 nm associated with the π - π^* transition, while two additional absorption peaks at 555 and 605 nm are contributed to the π - π stacking of P3HT chains.³⁸ The P3BT film also exhibits absorption peaks at about 510, 550 and 602 nm, and the peaks at 550 and 602 nm are contributed to crystalline P3BT. By increase of P3BT-nw content, the intensity of absorption peaks at about 510 and 550 nm reaches to the maximum at P3BT-nw weight percentage of 10 wt%. Moreover, the intensity of the absorption peak at about 605 nm contributing to P3HT becomes stronger upon the incorporation of P3BT-nw. According to Jenekhe,³⁸ the absorption peak at about 550 nm and 605 nm are characteristic to the crystalline P3HT. The crystallinity of P3HT is improved by P3BT-nw, which is consistent with the XRD result.

The photoluminescence spectra (**Figure 3c**) of P3HT:PCBM (black line) shows a strong PL emission peak at 638 nm assigned to the radiative decay of excitons to ground state. But the P3BT-nw shows a weak PL emission peak at 653 nm thanks to the easy transportation of nanowires causing the low opportunities of recombination of the photogenerated carrier. For the PL spectra of P3HT:P3BT-nw:PCBM films, the emission intensity decreases sharply as the content of P3BT-nw increases, suggesting that versatile heterojunction interfaces offer the multi-charge-transfer-channels for more efficient charge transfer. In addition, the surface morphology of the ternary blend films was characterized by atomic force microscope (AFM) as shown in **Figure S6**. The surface roughness continuously declined from 6.76 to 3.42 nm as the P3BT-nw content increasing from 0 wt% to 50 wt%.

Bulk heterojunction solar cells based on P3HT:P3BT-nw:PCBM films with various weight percentage of P3BT-nw were fabricated with a device structure (**Figure 4a**) of ITO/PEDOT:PSS/P3HT:P3BT-nw:PCBM/LiF/Al. **Figure 4b** presents the illuminated current-voltage (J - V) curves characteristics of the devices under AM1.5G (100 mW/cm²) light intensity illumination, and **Figure 4c** shows the J - V characteristics of PSCs based on the P3HT:P3BT-nw:PCBM that be measured without illumination.

Figure 4d exhibits the illuminated current-voltage ($J-V$) curves characteristics of the devices based on P3HT:P3BT:PCBM system for comparison. It is found that the leakage current of the device with P3BT-nw is considerably restrained, indicating that the recombination of carriers could be suppressed by P3BT-nw. Summary of the photovoltaic performance parameters are shown in **Table 2** and **Table 3**. The devices based on P3HT:PCBM has a PCE of 3.0%, with a short-circuit current (J_{sc}) of 7.79 mA/cm², an open circuit voltage (V_{oc}) of 0.597 V, a fill factor (FF) of 65.1%. By increase of the P3BT-nw content to 7 wt%, the PCE reaches to the highest value of 4.2% for the corresponding solar cell device. As expected, both of the J_{sc} and FF reach to the maximal value of 9.84 mA/cm² and 70.1%, respectively. In addition, the series resistance (R_s) decreases from 5.387 $\Omega\cdot\text{cm}^2$ to 2.506 $\Omega\cdot\text{cm}^2$ and the shut resistance (R_{sh}) from increases from 455.7 $\Omega\cdot\text{cm}^2$ to 8212 $\Omega\cdot\text{cm}^2$, in contrast to the pristine P3HT:PCBM device. Consequently, the reduced R_s and enhanced R_{sh} values contribute to the enhanced device performance by improving the J_{sc} and FF.⁴³ The variation of J_{sc} , V_{oc} , FF, and PCE values with P3BT-nw content is displayed in **Figure 5**, and it is observed that the V_{oc} shows of no significant change for the devices at P3BT-nw content below 10 wt%. However, the V_{oc} gradually decreases at P3BT-nw content above 25 wt%. Generally, the V_{oc} value depends on the energy difference between the highest occupied molecular orbital (HOMO) level of the donor and the lowest unoccupied molecular orbital (LUMO) level of the acceptor materials, as illustrated in Equation 2:⁴⁴

$$V_{oc} \approx E_{accepter}(LUMO) + E_{donor}(HOMO) + 0.3 \quad (2)$$

The depression of V_{oc} value at large amount of P3BT-nw should be due to the difference in the HOMO energy level between P3HT and P3BT. In contrast, the PCE value of the devices based on P3HT:P3BT:PCBM system gradually reduces from 3.0% to 1.3%, accompanying by the decrease of J_{sc} value. It is concluded that the improvement of the photovoltaic performance of the P3HT:PCBM system should be due to the incorporation of P3BT-nw. The existence of P3BT-nw in the active layer induces the crystallization of P3HT and provides multi-charge-transfer channels for

efficient charge transport, leading to the increase of J_{sc} value.

In order to evaluate the apparent charge carrier mobility in the active layer, $J^{0.5}$ - V characteristics of single charge carrier devices were measured using the space charge-limited-current (SCLC) model according to the Mott-Gurney equation:

$$J = (9/8)\mu\epsilon_0\epsilon_r(V^2/L^3) \quad (3)$$

where J is the current density, μ is the charge carrier mobility, ϵ_0 is the permittivity of free space (8.85×10^{-12} F m⁻¹), ϵ_r is the dielectric constant of P3HT or PCBM (assumed to 3), μ is carrier mobility, V is the applied voltage, and L is the film thickness.⁴⁵⁻⁴⁷

The thickness of the BHJ blend for SCLC measurement was about 120 nm. The $J^{0.5}$ - V characteristics of hole-only and electron-only devices are plotted in **Figure 6a** and **6b**, respectively. Summary of the carrier mobility that was fitted with the SCLC model was shown in **Table 4**. The apparent hole mobility reaches to the highest value of 7.90×10^{-4} cm²V⁻¹s⁻¹ at P3BT-nw content of 10 wt%, in contrast to 3.66×10^{-4} cm²V⁻¹s⁻¹ for the pristine P3HT:PCBM. The enhancement of the hole mobility is mainly contributed to the improved crystallization of P3HT induced by the P3BT-nw. In addition, the P3BT-nw are supposed to play the role of bridge between P3HT crystalline regions and offer multi-charge-transfer channels for more efficient charge transfer. However, the electron mobility always increases as the content of P3BT-nw increasing, and the pristine P3BT-nw:PCBM has the highest electron mobility which might be due to the increase of sizes of PCBM clusters as revealed by the GISAXS analysis (**Figure 8**). The results indicates that the addition of the P3BT-nw into the active layer can achieve an increase of both the electron and hole mobility and a more balanced charge transport in the devices.⁴⁸

To correlate the photovoltaic performance of the device with morphology of the active layer, the corresponding TEM images are shown in **Figure 7** and **Figure S7**. For the

pristine P3HT and P3BT specimens, in addition to the P3HT:P3BT blend (7 wt% P3BT), no characteristic morphology could be observed. In **Figure S7d**, the nanowires in the diameter of about 10 nm could be noticed for the P3HT:P3BT-nw blend. In addition, more dense nanowires are observed for the pristine P3BT-nw specimen as shown in **Figure S7e**. It is demonstrated that the nanowires could be obtained simply by blending of P3HT solution with P3BT-nw suspension, and the nanowires are found to be stable in the P3HT:P3BT-nw films. In the P3HT:PCBM blend, the phase-separated morphology with black PCBM clusters in the diameter of about 40-100 nm could be observed. However, no nanowires could be noticed in the TEM image. In the P3BT-nw:PCBM blend, the P3BT-nw in the diameter of about 8-10 nm are observed. These nanowires form an interconnected network surrounded by a continuous PCBM phase, forming a quasi-bicontinuous nanoscale morphology. Upon the incorporation of 7 wt% P3BT-nw into the P3HT:PCBM system, the morphology of the ternary blend shows of a significant change. The nanowires distributing in the matrix exhibit lower density and larger width as compared with the P3BT-nw:PCBM blend. Some of the nanowires seem to be covered by an additional layer, attributing to the P3HT phase.

Furthermore, GISAXS can give interpretations for structures across different lengths in the form of fractal sizes and provide more details on the hierarchical structures. We used the Fit GISAXS and IGOR Pro software to obtain the 2D and 1D profiles from GISAXS data,⁴⁹ as shown in **Figure 8**. Extracting quantitative information from GISAXS profiles is extremely challenging given the irregularly shaped, polydisperse, interconnected and randomly distributed domains characteristic of a BHJ morphology.¹⁹ There exists no widely accepted GISAXS model for BHJ PSCs blends, although Su et al. have successfully used the Debye-Anderson-Brumberger (DAB) model and the polydisperse hard sphere model to describe the cluster size and distribution of PCBM domains.⁵⁰ Therefore, we elect to interpret the data qualitatively based on the analysis of the intensity variation of the profiles. It is observed that the as-cast P3HT:PCBM film exhibit a power-law dependence of 2 and do not show

obvious Guinier regime, both indicating that the domains are poorly phase segregated (i.e., highly intermixed) with no well-defined domain sizes within the length scales probed. However, the P3HT:P3BT-nw:PCBM (0.93:0.07:1) and P3BT-nw:PCBM films shows of a discernible shoulder at about 0.25 nm^{-1} , and the power-law exponent increases to higher values. These features indicate that phase-segregation takes place during solvent evaporation process, and the PCBM molecules tend to aggregate into larger PCBM clusters in the presence of P3BT-nw which may facilitate the electron transport as revealed by the SCLC analysis.

Based on the above analysis, a model describes the morphology of the ternary blend is illustrated in **Figure 9**. The P3BT-nw could serve as the template to induce the heterogeneous crystallization of P3HT and play the role of bridge to connect the separated crystalline domains of P3HT, in addition to induce the aggregation of PCBM molecules into bigger clusters. Therefore, the enhanced photovoltaic performance and hole and electron mobilities should be contributing to the optimized morphology of the active layer upon incorporation of P3BT-nw.

Conclusions

The P3BT-nw were incorporated into the P3HT:PCBM system via the solution blending method. As revealed by XRD, GIXRD and DSC analysis, the existence of P3BT-nw could induce the crystallization of P3HT. The P3BT-nw played the role of bridge connecting the different P3HT crystalline regions to offer multi-charge-transfer channels for more efficient charge separation and transfer, which eventually led to the improvement of photovoltaic performance. The PCE value of the device could reach to the highest value of 4.2%, in contrast to the pristine P3HT:PCBM system of 3.0% and the P3HT:P3BT:PCBM systems ranging from 1.3% to 3.1%. The addition of the P3BT-nw into the active layer could lead to an increase of both the electron and hole mobility and a more balanced charge transport in the devices, as well as enhancement of light absorption. Moreover, the P3BT-nw are supposed to induce the PCBM molecules to form bigger clusters.

Electronic supplementary information (ESI) available.

Acknowledgements

The financial supports for this work are provided by the National Natural Science Foundation of China (51273088, and 51303077), Doctoral Programs Foundation of Ministry of Education of China (Grants 20123601120010), and Fund by State Key Laboratory of Luminescent Materials and Devices (Grants 2013-skllmd-04). The experiments are partially carried out in Shanghai Synchrotron Radiation Facility (SSRF), and we also thank the team in SSRF for supporting during the GISAXS measurement. We thank Professor Qiu Dong in the Institute of Chemistry, Chinese Academy of Sciences for his helpful discussion in the analysis of the experimental data.

References

- (1) Yu, G.; Gao, J.; Hummelen, J. C.; Wudl, F.; Heeger, A. J. *Science*, 1995, **270**, 1789.
- (2) Dennler, G.; Scharber, M. C.; Brabec, C. J. *Adv. Mater.*, 2009, **21**, 1323.
- (3) Li, G.; Zhu, R.; Yang, Y. *Nat. Photon.*, 2012, **6**, 153.
- (4) You, J.; Dou, L.; Yoshimura, K.; Kato, T.; Ohya, K.; Moriarty, T.; Emery, K.; Chen, C. C.; Gao, J.; Li, G.; Yang, Y. *Nat. Commun.*, 2013, **4**, 1446.
- (5) Yang, T.; Wang, M.; Duan, C.; Hu, X.; Huang, L.; Peng, J.; Huang, F.; Gong, X. *Energy Environ. Sci.*, 2012, **5**, 8208.
- (6) You, J.; Chen, C. C.; Hong, Z.; Yoshimura, K.; Ohya, K.; Xu, R.; Ye, S.; Gao, J.; Li, G.; Yang, Y. *Adv. Mater.*, 2013, **25**, 3973.
- (7) Chen, H.-Y.; Hou, J.; Zhang, S.; YongyeLiang; Yang, G.; Yang, Y.; Yu, L.; YueWu; Li, G. *Nat. Photon.*, 2009, **3**, 649.
- (8) Beaujuge, P. M.; Frechet, J. M. J. *Am. Chem. Soc.*, 2011, **133**, 20009.
- (9) Li, Y. *Acc. Chem. Res.*, 2012, **45**, 723.
- (10) Yip, H.-L.; Jen, A. K. Y. *Energ. Environ. Sci.*, 2012, **5**, 5994.
- (11) Ameri, T.; Li, N.; Brabec, C. J. *Energ. Environ. Sci.*, 2013, **6**, 2390.
- (12) Po, R.; Carbonera, C.; Bernardi, A.; Camaioni, N. *Energ. Environ. Sci.*, 2011, **4**, 285.
- (13) He, Z.; Zhong, C.; Su, S.; Xu, M.; Wu, H.; Cao, Y. *Nat. Photon.*, 2012, **6**, 591.
- (14) Roncali, J.; Leriche, P.; Blanchard, P. *Adv. Mater.*, 2014, **26**, 3821.
- (15) Li, G.; Shrotriya, V.; Huang, J.; Yao, Y.; Moriarty, T.; Emery, K.; Yang, Y. *Nat. Mater.*, 2005, **4**, 864.
- (16) Kim, Y.; Cook, S.; Tuladhar, S. M.; Choulis, S. A.; Nelson, J.; Durrant, J. R.; Bradley, D. D. C.; Giles, M.; McCulloch, I.; Ha, C. S.; Ree, M. *Nat. Mater.*, 2006, **5**, 197.
- (17) Ma, W. L.; Yang, C. Y.; Gong, X.; Lee, K.; Heeger, A. J. *Adv. Funct. Mater.*, 2005, **15**, 1617.
- (18) Liu, H. W.; Chang D.Y.; Chiu, W. Y.; Rwei, S. P.; Wang, L. *J. Mater. Chem.*, 2012, **22**, 15586.
- (19) Sharenko, A.; Kuik, M.; Toney, M. F.; Nguyen, T. Q. *Adv. Funct. Mater.*, 2014, **24**, 3543.
- (20) Chen, H.; Hsiao, Y. C.; Hu, B.; Dadmun, M. *Adv. Funct. Mater.*, 2014, DOI: 10.1002/adfm.201400552.
- (21) Zhang, F.; Jespersen, K. G.; Björström, C.; Svensson, M.; Andersson, M. R.; Sundström, V. Magnusson, K. Moons, E.; Yartsev, A.; Inganäs, O. *Adv. Funct. Mater.*, 2006, **16**, 667.
- (22) Chen, Y.; Zhang, S.; Wu, Y.; Hou, J. *Adv. Mater.*, 2014, **26**, 2744.
- (23) Yang, C.; Lee, J. K.; Heeger, A. J.; Wudl, F. *J. Mater. Chem.*, 2009, **19**, 5416.
- (24) Sivula, K.; Ball, Z. T.; Watanabe, N.; Fréchet, J. M. J. *Adv. Mater.*, 2006, **18**, 206.
- (25) Idé, J.; Méreau, R.; Ducasse, L.; Castet, F.; Bock, H.; Olivier, Y.; Cornil, J.; Beljonne, D.; D'Avino, G.; Roscioni, O. M.; Muccioli, L.; Zannoni, C. *J. Am. Chem. Soc.*, 2014, **136**, 2911.

- (26) Machui, F.; Rathgeber, S.; Li, N.; Ameri, T.; Brabec, C. J. *J. Mater. Chem.*, 2012, **22**, 15570.
- (27) Chen, G.; Sasabe, H.; Wang, Z.; Wang, X. F.; Hong, Z.; Yang, Y.; Kido, J. *Adv. Mater.*, 2012, **24**, 2768.
- (28) Honda, S.; Nogami, T.; Ohkita, H.; Bente, H.; Ito, S. *ACS Appl. Mater. Interfaces*, 2009, **4**, 804.
- (29) Liao, H. C.; Tsao, C. S.; Lin, T. H.; Jao, M. H.; Chuang, C. M.; Chang, S. Y.; Huang, Y. C.; Shao, Y. T.; Chen, C. Y.; Su, C. J.; Jeng, U. S.; Chen, Y. F.; Su, W. F. *ACS Nano*, 2012, **6**, 1657.
- (30) Kwon, S.; Yu, K.; Kweon, K.; Kim, G.; Kim, J.; Kim, H.; Jo, Y. R.; Kim, B. J.; Kim, J.; Lee, S. H.; Lee, K. *Nat. Commun.*, 2014, **5**, 4183.
- (31) Yang, H.; Shin, T. J.; Yang, L.; Cho, K.; Ryu, C. Y.; Bao, Z. *Adv. Funct. Mater.*, 2005, **15**, 671.
- (32) Zhang, R.; Li, B.; Iovu, M. C.; Jeffries-El, M.; Sauv e, G.; Cooper, J.; Jia, S.; Tristram-Nagle, S.; Smilgies, D. M.; Lambeth, D. N.; McCullough, R. D.; Kowalewski, T. *J. Am. Chem. Soc.*, 2006, **128**, 3480.
- (33) Oh, J. Y.; Shin, M.; Lee, T. I.; Jang, W. S.; Min, Y.; Myoung, J. M.; Baik, H. K.; Jeong, U. *Macromolecules*, 2012, **45**, 7504.
- (34) Li, L.; Lu, G.; Yang, X. *J. Mater. Chem.*, 2008, **18**, 1984.
- (35) Aiyar, A. R.; Hong, J. I.; Nambiar, R.; Collard, D. M.; Reichmanis, E. *Adv. Funct. Mater.*, 2011, **21**, 2652.
- (36) Kim, B. G.; Kim, M. S.; Kim, J. *ACS Nano*, 2010, **4**, 2160.
- (37) Chang, M.; Lee, J.; Kleinhenz, N.; Fu, B.; Reichmanis, E. *Adv. Funct. Mater.*, 2014, **24**, 4457.
- (38) Xin, H.; Kim, F. S.; Jenekhe, S. A. *J. Am. Chem. Soc.*, 2008, **130**, 5424.
- (39) Xin, H.; Reid, O. G.; Ren, G.; Kim, F. S.; Ginger, D. S.; Jenekhe, S. A. *ACS Nano*, 2010, **4**, 1861.
- (40) Xin, H.; Ren, G.; Kim, F. S.; Jenekhe, S. A. *Chem. Mater.*, 2008, **20**, 6199.
- (41) Methods of X-Ray and Neutron Scattering in Polymer Science (Ed: R. J. Roe), Oxford University Press, Inc., UK 2000.
- (42) Keith, H. D.; Padden, F. J. *J. Appl. Phys.*, 1964, **35**, 1270.
- (43) Liang, Z.; Zhang, Q.; Wiranwetchayan, O.; Xi, J.; Yang, Z.; Park, K.; Li, C.; Cao, G. *Adv. Funct. Mater.*, 2012, **22**, 2194.
- (44) Heeger, A. J. *Adv. Mater.*, 2013, **26**, 10.
- (45) Chen, H. C.; Lai, C. W.; Wu, I. C.; Pan, H. R.; Chen, I. W.; Peng, Y. K.; Liu, C. L.; Chen, C. H.; Chou, P. T. *Adv. Mater.*, 2011, **23**, 5451.
- (46) Cheng, Y.-J.; Hsieh, C.-H.; Li, P.-J.; Hsu, C.-S. *Adv. Funct. Mater.*, 2011, **21**, 1723.
- (47) Liu, Y.; Wan, X.; Wang, F.; Zhou, J.; Long, G.; Tian, J.; Chen, Y. *Adv. Mater.*, 2011, **23**, 5387.
- (48) He, Z.; Zhong, C.; Huang, X.; Wong, W. Y.; Wu, H.; Chen, L.; Su, S.; Cao, Y. *Adv. Mater.*, 2011, **23**, 4636.
- (49) Babonneau D. *J. Appl. Crystallogr.*, 2010, **43**, 929.
- (50) Liao, H. C.; Tsao, C. S.; Lin, T. H.; Chuang, C. M.; Chen, U. S. J.; Su, C. H.;

Chen, Y. Y.; Su, W. F. *J. Am. Chem. Soc.*, 2011, **133**, 13064.

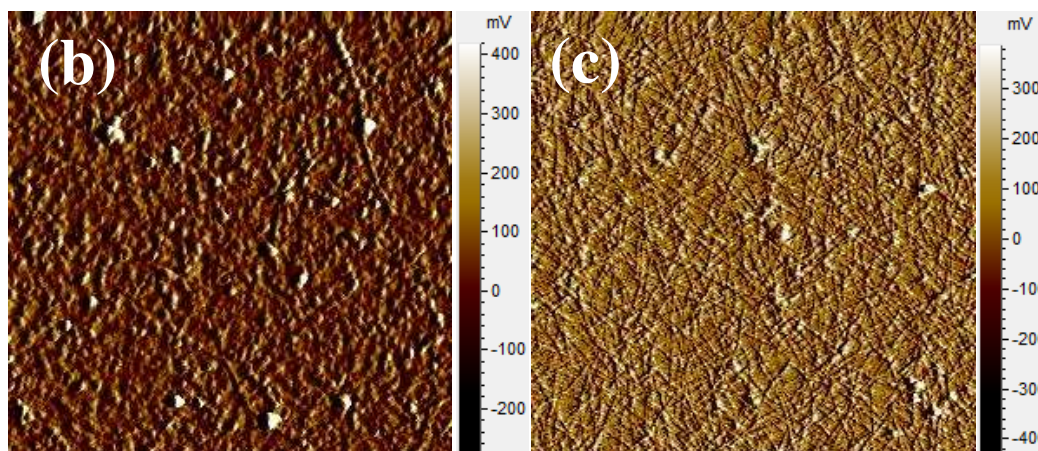
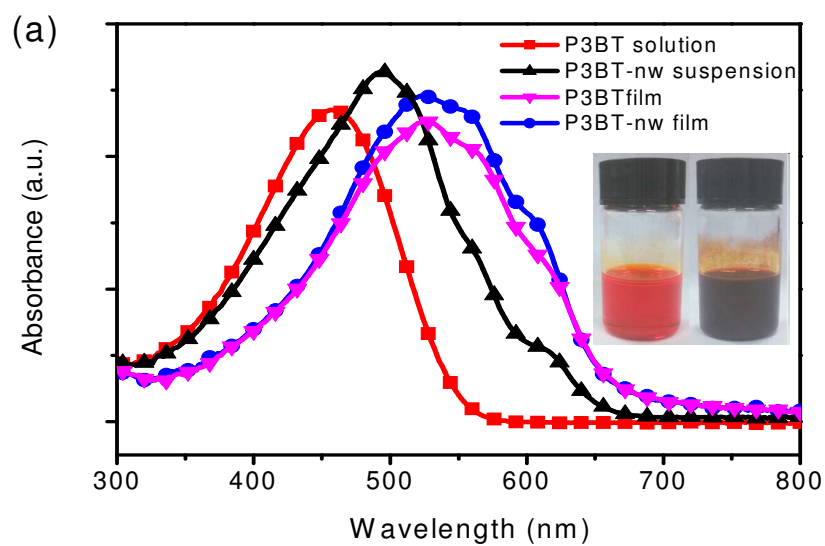
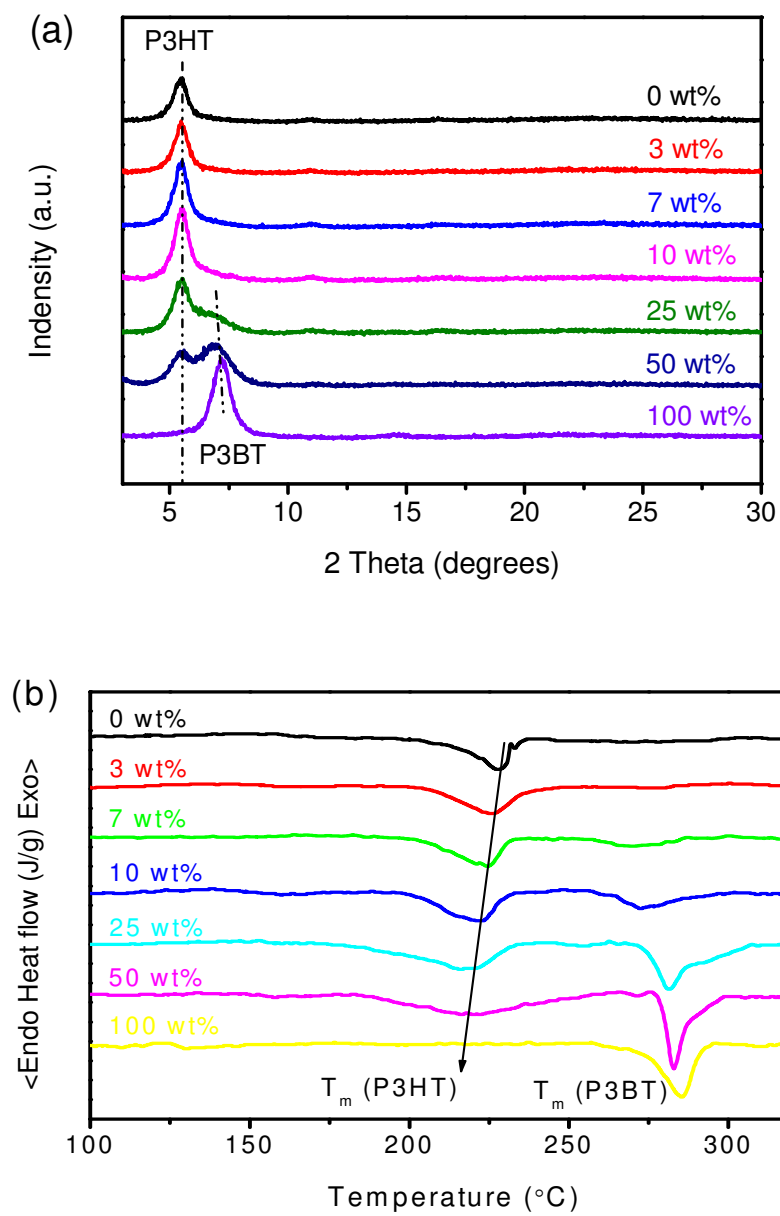


Figure 1. (a) The UV-vis absorption profiles of P3BT and P3BT-nw in solution and solid film state, and the inset is photograph of P3BT and P3BT-nw in ODCB solution, respectively. The AFM amplitude images of (b) P3BT and (c) P3BT-nw films. The scan areas are $5 \times 5 \mu\text{m}$.



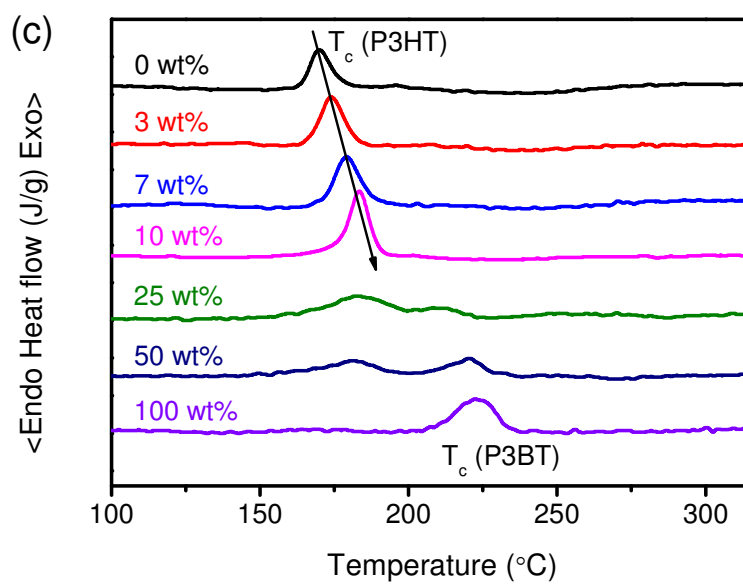
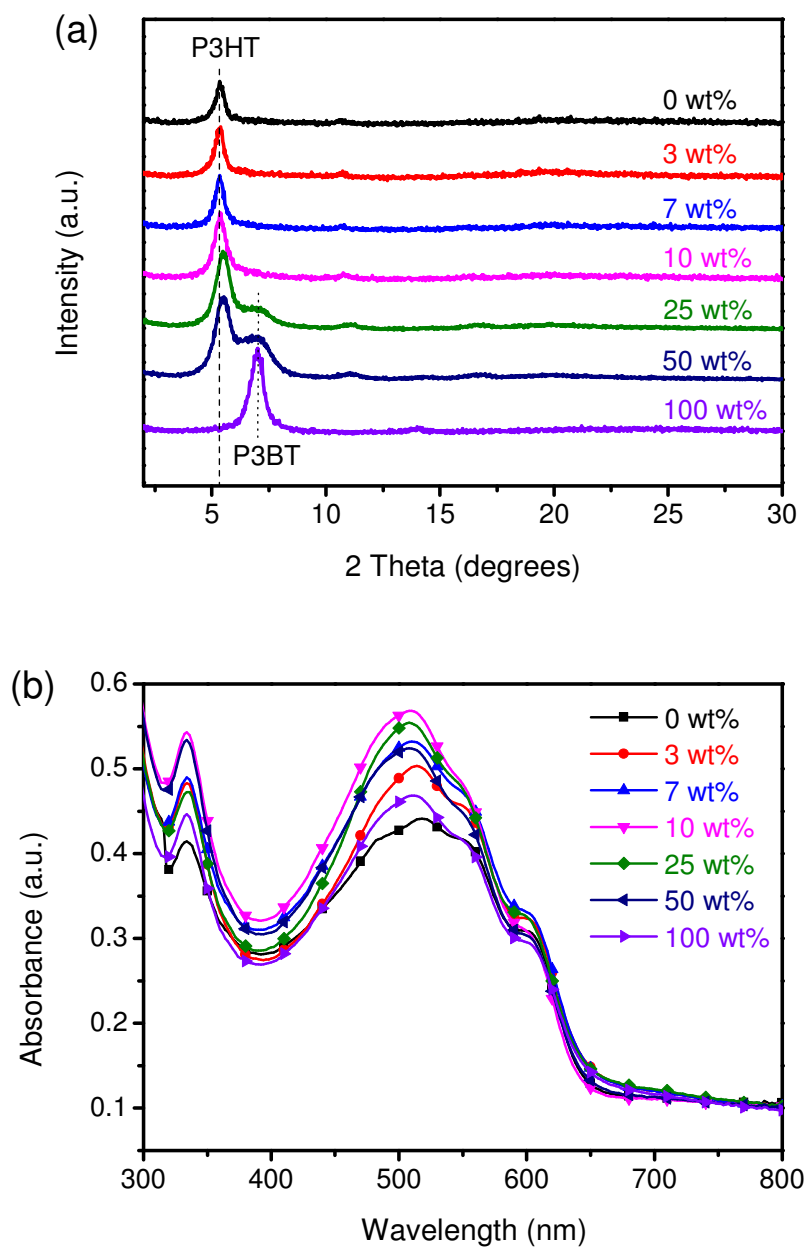


Figure 2. (a) X-ray spectra, DSC (b) heating and (c) cooling curves of P3HT:P3BT-nw blends at different weight percentage of P3BT-nw.



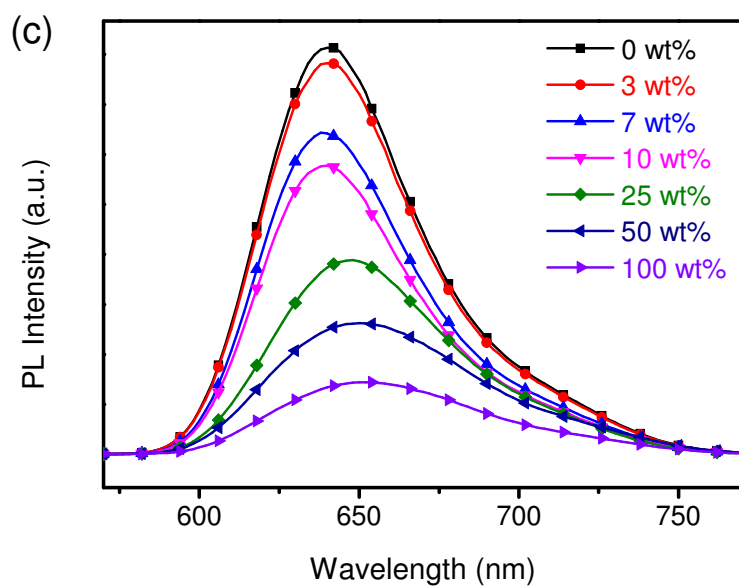
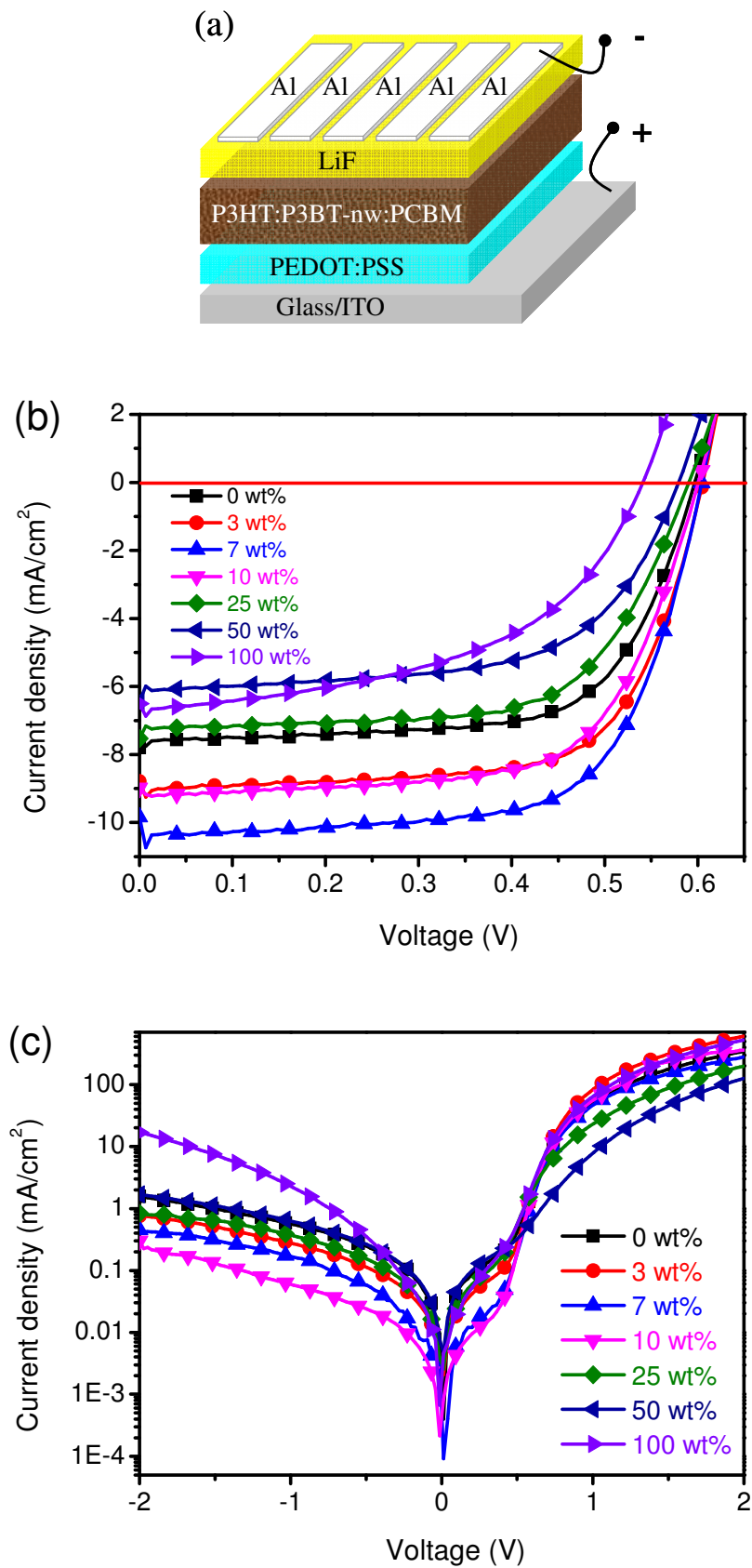


Figure 3. (a) X-ray spectra, (b) UV-visible absorption spectra and (c) PL spectra of the thin films of P3HT:PCBM blends with various weight percentage of P3BT-nw.



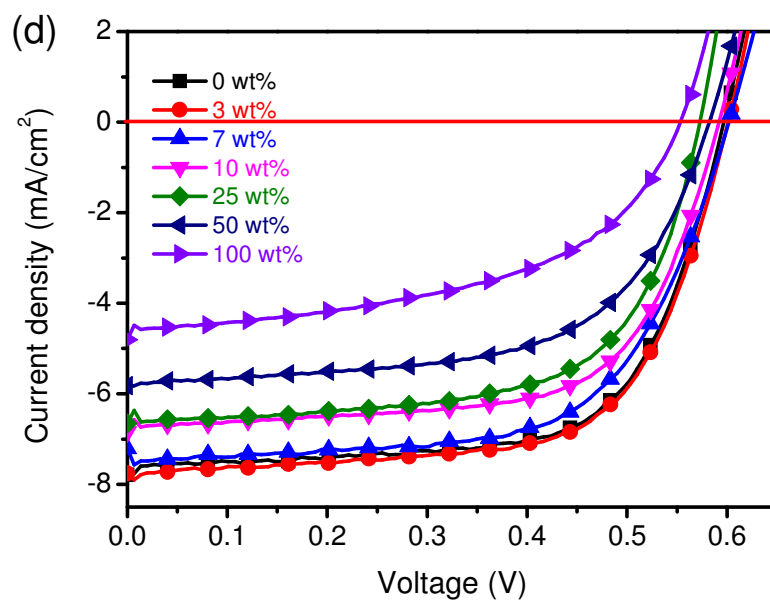


Figure 4. (a) Device structure of the solar cell, (b) current-voltage (J - V) characteristics and (c) dark current-voltage (J - V) characteristics of solar cells based on P3HT:PCBM blends with various weight percentage of P3BT-nw, and (d) current-voltage (J - V) characteristics of solar cells based on P3HT:PCBM blends with various weight percentage of P3BT.

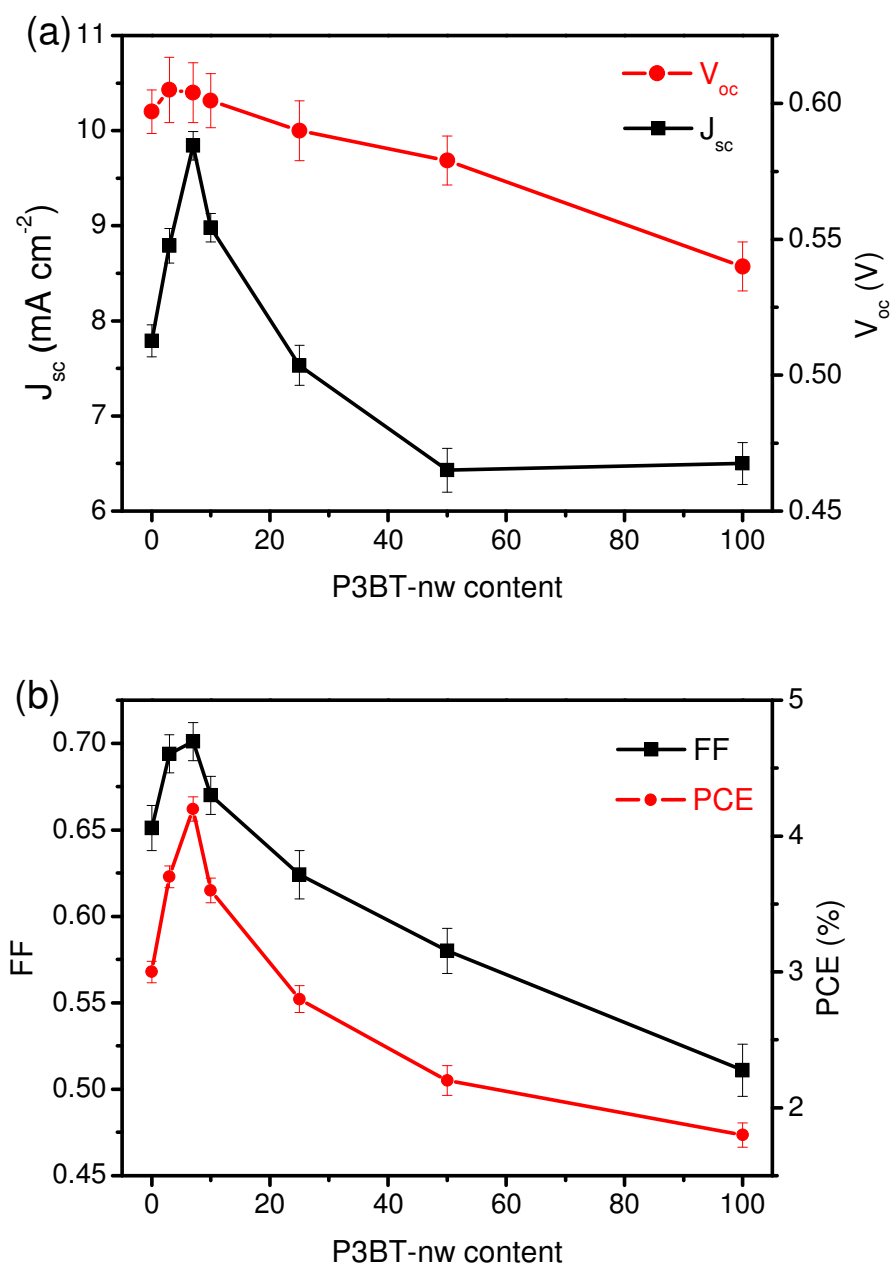


Figure 5. Relationship of (a) short-circuit current density and open-circuit voltage, and (b) fill factor and power conversion efficiency with P3BT-nw content in P3HT:PCBM blends.

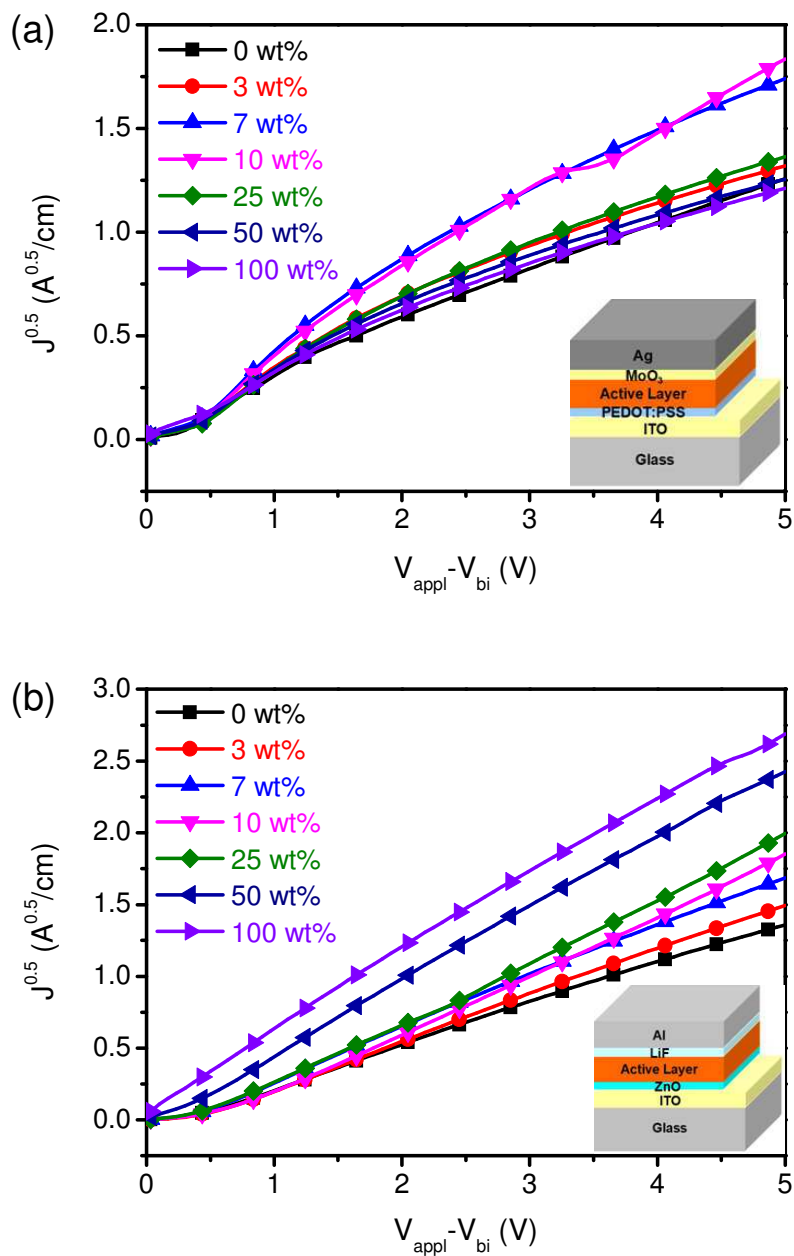


Figure 6. $J^{0.5}$ - V characteristics of (a) hole-only and (b) electron-only devices with various weight percentage of P3BT-nw.

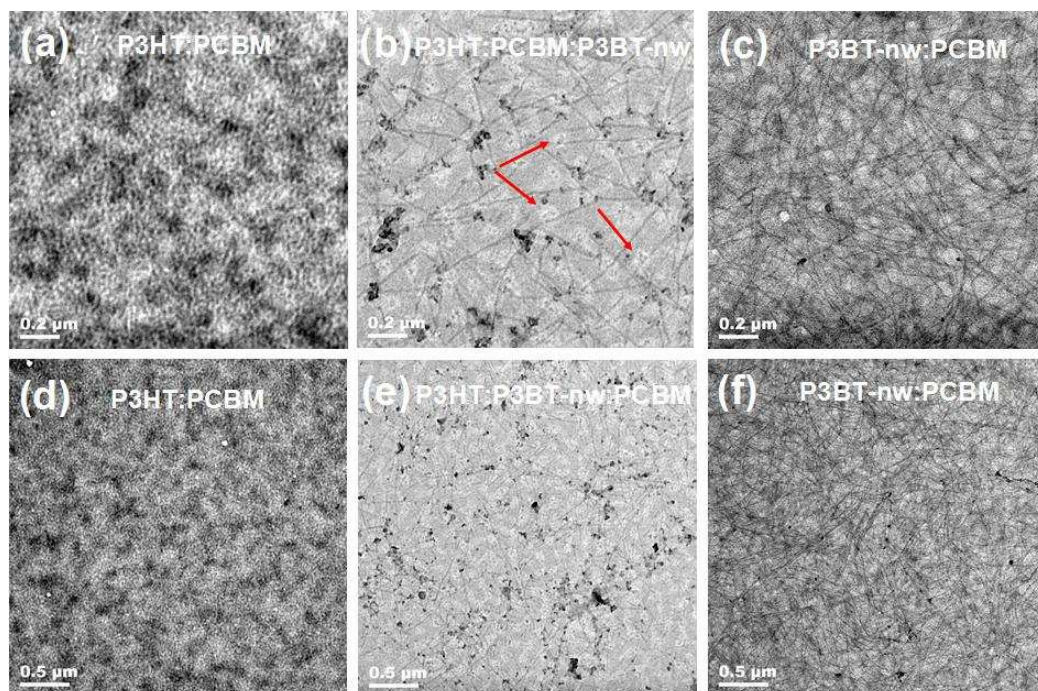


Figure 7. TEM graphs of the active layer films of (a, d) P3HT:PCBM, (b, e) P3HT:PCBM with 7 wt% P3BT-nw, and (c, f) P3BT-nw:PCBM under different proportion. The red arrows indicate the formation of one additional layer on the P3BT-nw.

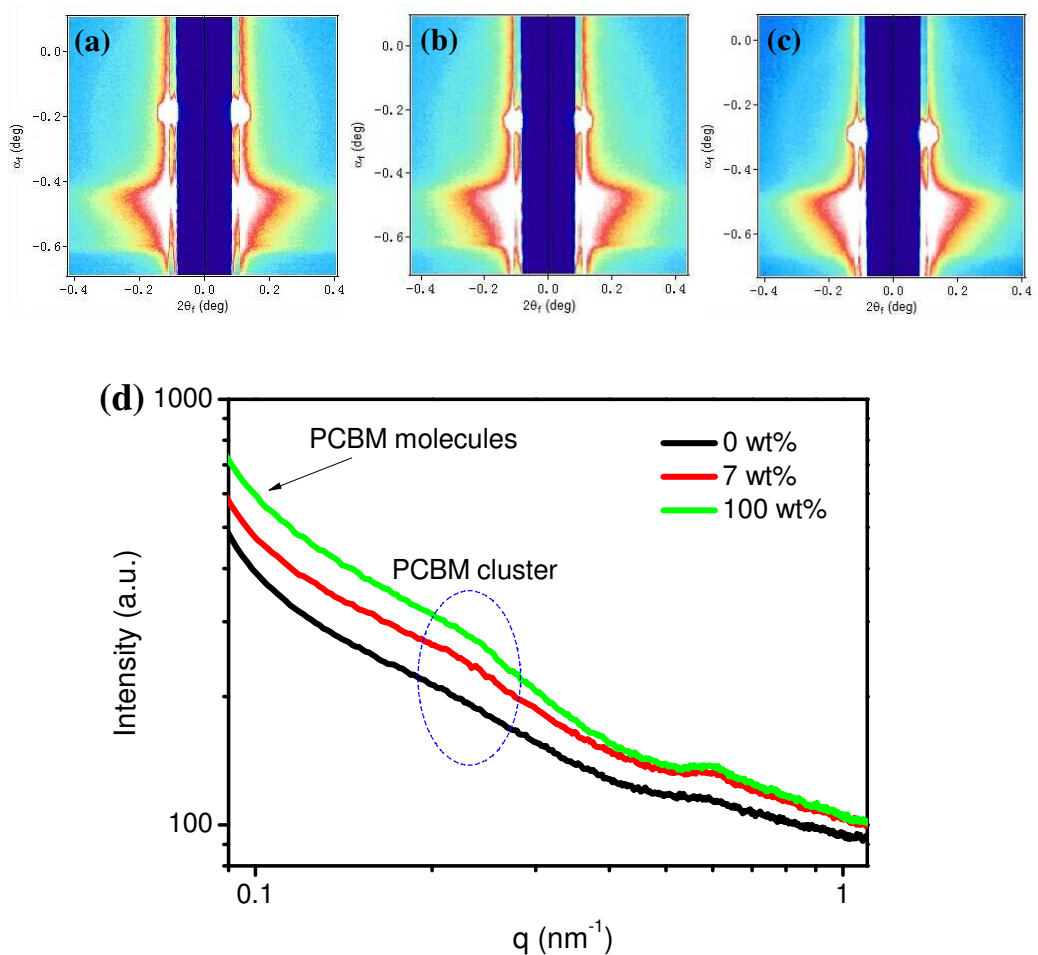


Figure 8. Two-dimensional GISAXS images of (a) P3HT:PCBM, (b) P3HT:P3BT-nw(7 wt%):PCBM and (c) P3BT-nw:PCBM films, and (d) selected GISAXS profiles measured for the P3HT:PCBM, P3HT:P3BT-nw (7 wt%):PCBM and P3BT-nw:PCBM films.

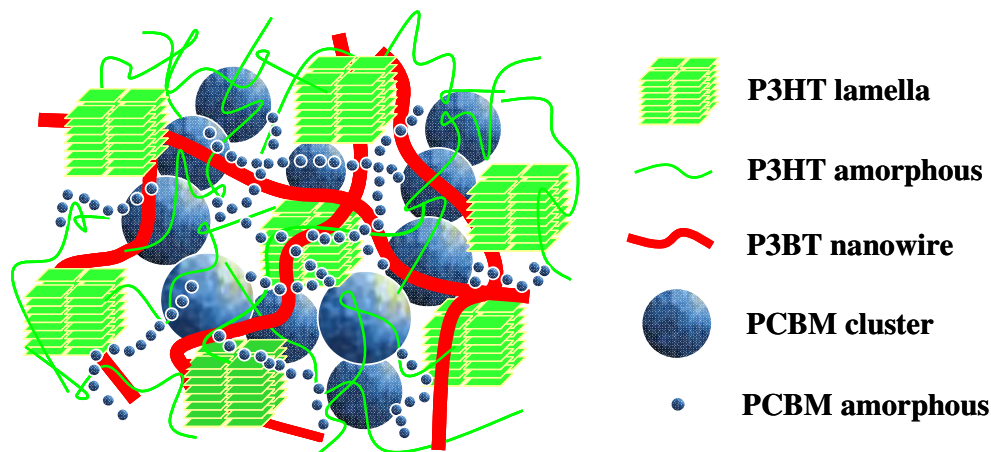


Figure 9. Schematic representation of the spatial arrangement of P3HT lamella, P3HT amorphous domains, P3BT-nw, PCBM clusters and PCBM molecules in the phase-separated BHJ morphology of P3HT:P3BT-nw:PCBM ternary blended film. The P3BT-nw-tuned nanostructure provides interconnected pathways for efficient long-range charge transport.

Table 1. The data of the melting temperature (T_m), melting enthalpy (ΔH_m), crystallization temperature (T_c) and crystallization enthalpy (ΔH_c) for P3HT and P3BT-nw blends.

P3BT-nw content (wt%)	T_m (P3HT) (°C)	ΔH_m (P3HT) (J/g)	T_m (P3BT) (°C)	ΔH_m (P3BT) (J/g)	T_c (P3HT) (°C)	ΔH_c (P3HT) (J/g)	T_c (P3BT) (°C)	ΔH_c (P3BT) (J/g)
0	228.4	8.5			170.1	7.1		
3	227.0	9.0			173.8	9.3		
7	224.7	8.9	270.1	3.9	178.1	10.4		
10	222.3	12.4	272.6	5.0	182.8	11.3		
25	219.0	12.8	282.1	9.7	182.4	6.3	214.3	1.2
50	218.1	13.0	283.4	10.1	181.8	3.4	220.9	4.6
100			285.8	10.4			223.3	8.0

Table 2. Summary of the photovoltaic performance of P3HT:PCBM solar cells with various weight percentage of P3BT-nw under AM 1.5G solar illumination.

P3BT-nw content (wt%)	J_{sc} (mA/cm ²)	V_{oc} (V)	FF (%)	PCE (%)	R_s ($\Omega \cdot \text{cm}^2$)	R_{sh} ($\Omega \cdot \text{cm}^2$)
0	7.79	0.597	65.1	3.0	5.38	455.7
3	8.79	0.605	69.4	3.7	2.44	869.8
7	9.84	0.604	70.1	4.2	2.50	8212
10	8.98	0.601	67.0	3.6	4.69	3861
25	7.53	0.590	62.4	2.8	18.66	645.3
50	6.43	0.579	58.0	2.2	15.19	453.2
100	6.50	0.540	51.1	1.8	3.34	381.1

Table 3. Summary of the photovoltaic performance of P3HT:PCBM solar cells with various weight percentage of P3BT under AM 1.5G solar illumination.

P3BT content (wt%)	J_{sc} (mA/cm ²)	V_{oc} (V)	FF (%)	PCE (%)	R_s ($\Omega \cdot \text{cm}^2$)	R_{sh} ($\Omega \cdot \text{cm}^2$)
0	7.79	0.597	65.1	3.0	5.38	455.7
3	7.76	0.601	65.6	3.1	47.88	529.1
7	7.21	0.602	65.4	2.8	5.98	1597
10	6.84	0.592	64.2	2.6	24.96	1137
25	6.65	0.573	63.6	2.4	24.00	2403
50	5.82	0.582	60.2	2.0	3.36	644.6
100	4.81	0.553	49.0	1.3	21.04	480.6

Table 4. Summary of the carrier mobility of the P3HT:PCBM device with various weight percentage of P3BT-nw.

P3BT-nw content (wt%)	Hole mobility ($\text{cm}^2/\text{V}\cdot\text{s}$) ^a	Electron mobility ($\text{cm}^2/\text{V}\cdot\text{s}$) ^b
0	3.66×10^{-4}	4.86×10^{-4}
3	4.12×10^{-4}	5.97×10^{-4}
7	7.38×10^{-4}	7.41×10^{-4}
10	7.90×10^{-4}	8.88×10^{-4}
25	4.52×10^{-4}	9.98×10^{-4}
50	3.70×10^{-4}	1.47×10^{-3}
100	3.33×10^{-4}	1.63×10^{-3}

^a Hole-only device configuration: ITO/PEDOT:PSS/P3HT:P3BT-nw:PCBM/MoO₃/Ag.

^b Electron-only device configuration: ITO/ZnO/P3HT:P3BT-nw:PCBM/LiF/Al.

Highlights**Poly(3-butylthiophene) Nanowires Inducing Crystallization of Poly(3-hexylthiophene) Nanowires Inducing Crystallization of Poly(3-hexylthiophene) for Enhanced Photovoltaic Performance**

Lin Zhang, Weihua Zhou*, Jiangman Shi, Ting Hu, Xiaotian Hu, Yong Zhang,
Yiwang Chen

The P3BT nanowires induce the crystallization of P3HT and the aggregation of PC₆₁BM molecules, facilitating charge transportation.

